AIP | Journal of Applied Physics

Trap modulated photoresponse of InGaN/Si isotype heterojunction at zero-bias

Greeshma Chandan, Shruti Mukundan, Lokesh Mohan, Basanta Roul, and S. B. Krupanidhi

Citation: Journal of Applied Physics **118**, 024503 (2015); doi: 10.1063/1.4926480
View online: http://dx.doi.org/10.1063/1.4926480
View Table of Contents: http://scitation.aip.org/content/aip/journal/jap/118/2?ver=pdfcov
Published by the AIP Publishing

Trap modulated photoresponse of InGaN/Si isotype heterojunction at zero-bias

Greeshma Chandan,[1] Shruti Mukundan,[1] Lokesh Mohan,[1] Basanta Roul,[1,2] and S. B. Krupanidhi[1,a)]
[1]*Materials Research Centre, Indian Institute of Science, Bangalore, India*
[2]*Central Research Laboratory, Bharat Electronics, Bangalore, India*

(Received 14 January 2015; accepted 27 June 2015; published online 9 July 2015)

n-n isotype heterojunction of InGaN and bare Si (111) was formed by plasma assisted molecular beam epitaxy without nitridation steps or buffer layers. High resolution X-ray diffraction studies were carried out to confirm the formation of epilayers on Si (111). X-ray rocking curves revealed the presence of large number of edge threading dislocations at the interface. Room temperature photoluminescence studies were carried out to confirm the bandgap and the presence of defects. Temperature dependent *I-V* measurements of Al/InGaN/Si (111)/Al taken in dark confirm the rectifying nature of the device. *I-V* characteristics under UV illumination, showed modest rectification and was operated at zero bias making it a self-powered device. A band diagram of the heterojunction is proposed to understand the transport mechanism for self-powered functioning of the device.
 [http://dx.doi.org/10.1063/1.4926480]

I. INTRODUCTION

When two different semiconductors of same type are brought into close contact, the resulting heterojunction is often referred to as n-n or p-p isotype heterojunction depending on the type of semiconductors chosen. Although most of the semiconductor devices have p-n junction as the backbone, n-n heterojunctions have also found use in different applications such as photodetectors,[1,2] light emitting diodes,[3] solar cells,[4] and injection lasers.[5] Unlike in p-n junction, the charge carriers are predominantly either electrons in n-n isotype or holes in p-p isotype semiconductor junctions. However, due to large effective mass of holes than electrons, their mobility is very less and thus a p-p isotype junction is not preferred for high speed electronic applications. So far, the most extensively studied material systems are ZnO/Si,[1,6] $In_xGa_{1-x}As$, $In_xGa_{1-x}Sb$,[7] Ge-Si,[2] etc. Very few groups have reported studies on isotype heterojunctions of $In_xGa_{1-x}N$ system.[8,9] The replacement of toxic elements, such as arsenic and antimony with nitrogen and the tunability of this system from near infrared (for $x = 1$) to ultraviolet region (for $x = 0$), gives it an edge over the other material systems for high speed optoelectronic applications. Nevertheless, the large lattice mismatch of InGaN with silicon substrates has hindered the realization of silicon based commercial devices and is limited to sapphire which happens to be an insulator. The integration of InGaN based devices on silicon, where silicon processing being a well-endowed and matured semiconductor technology, opens the doors to wide range of applications. Therefore, obtaining smooth and abrupt heterojunctions with minimum density of interface defects by overcoming the lattice mismatch issue has been a concern of great interest for many researchers across the globe. The advancements in epitaxial fabrication techniques over the time have allowed researchers to address such critical problems with a lot of ease in recent times. Plasma assisted molecular beam epitaxy has been one of the most successful techniques for growing smooth and abrupt heterojunctions with atomic level precision, and also one can achieve film thickness of the order of few monolayers, at very low growth temperatures compared to other techniques.

With the depleting non-renewable energy resources and renewable energy technologies being in a budding stage, energy has become a primary concern in today's life. Therefore, small, energy efficient, and low power consuming devices are on high demand and have gained much attention in recent times, especially in the semiconductor industry. Several attempts have been made to demonstrate low power consuming or self-powered photodetectors.[10,11] There are a few reports on the UV photodetection using InGaN as an active layer.[12,13] Previously, our group has reported electrical studies on a similar heterojunction;[14] however, to the best of our knowledge, no previous reports exist on Al/n-$In_{0.15}GaN_{0.85}$/n-Si(111)/Al isotype heterojunctions' voltage dependent photoresponse under on-off conditions of UV radiation. In this work, we report the development of a UV photodetector which is operated at zero bias. The device comprises a simple n-InGaN/n-Si heterojunction. The role of interface defects originating due to the large lattice mismatch, such as traps, in modulating the built-in electric field driven photoresponse has been discussed.

II. EXPERIMENTAL DETAILS

The n-Si (111) substrates of $1 \times 1\,cm^2$ in size were cleaned chemically by tri-chloroethylene, acetone, and methanol and were dipped in 5% HF for 60 s to remove the native oxide prior to loading in a RF-MBE chamber (OMICRON). A Radio Frequency (RF) plasma source from Oxford Scientific (RF OSPrey) with a frequency of 13.56 MHz was

a)Author to whom correspondence should be addressed. Electronic mail: sbk@mrc.iisc.ernet.in. Tel.: 91-80-2360 1330. Fax: +91-80-2360 7316.

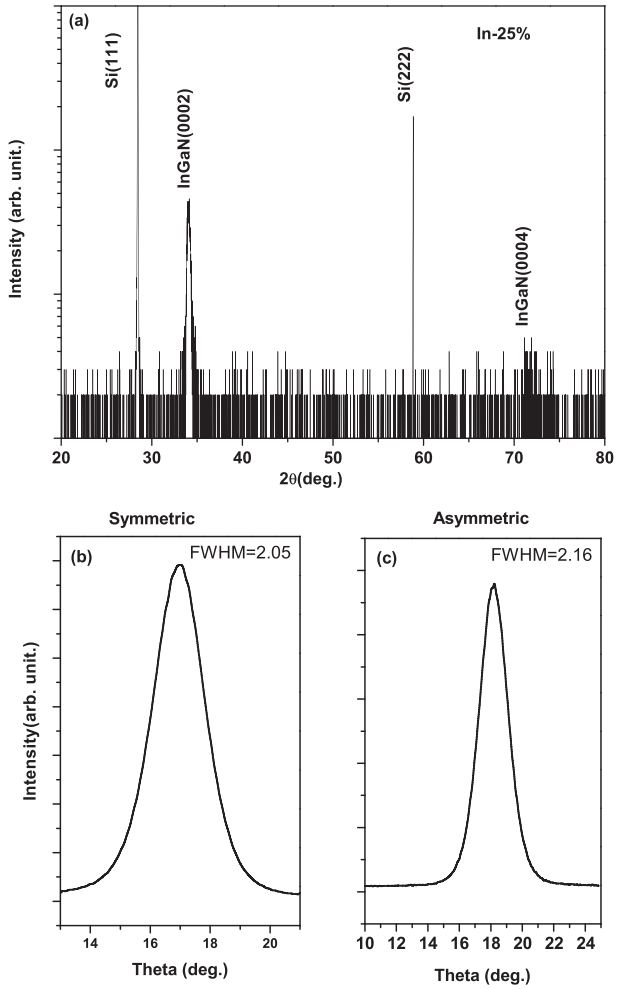

FIG. 1. (a) HRXRD $2\theta-\omega$ scan of InGaN on bare Si (111), X-ray rocking curve of (b) (002) and (c) (105) reflections.

used to obtain the nitrogen plasma. Thermal cleaning of Si (111) is a crucial step to obtain a smoother surface prior to growth without any residual oxide layer. Therefore, to ensure the complete removal of SiO_2 layer, thermal cleaning was carried out at 900 °C. The substrate temperature was further reduced to 550 °C and growth was carried out for 2 h without any intermediate steps. The Indium (In) beam equivalent pressure (BEP), Gallium (Ga) BEP, nitrogen flow, and plasma power were kept at 8.52×10^{-8} mbar, 1.2×10^{-7} mbar, 1 sccm, and 350 W, respectively. A part of InGaN film was subjected to Reactive ion etching (RIE, Anelva) until the Si substrate was exposed for ohmic contact. Circular aluminum contacts with diameters of 600 μm were then deposited by thermal evaporation on the InGaN film and Si (111) substrate with the help of a physical mask. Later, the fabricated devices were annealed in vacuum for better contact formation. The structural characterizations were carried out on Bruker Discover D8 four circle high resolution X-Ray diffractometer (HRXRD). Photoluminescence (PL) spectra were taken in a HR Labram micro Photoluminescence spectrometer. TEM studies were carried out in JEM 2100F. TEM lamella preparation was prepared in the FEI Quanta 3DFEG dual beam system. The temperature dependent current-voltage and photoresponse measurements were obtained on a

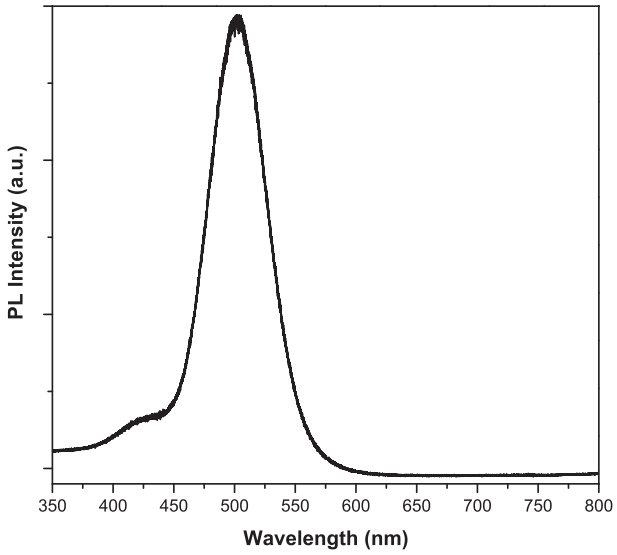

FIG. 2. Room temperature PL spectra of InGaN on Si (111).

homebuilt vacuum chamber integrated with Keithley 2400 Source Measure Unit. Hall measurements were carried out by HMS 5000 Hall measurement system from Ecopia. A handheld lamp emitting long UV-A radiation ranging from 380 nm to 310 nm and power density of 0.3 mW/m^2 was used as UV radiation source for photoresponse experiments.

III. RESULTS AND DISCUSSION

Figure 1(a) shows the 2θ-ωHRXRD scan of InGaN epilayers on Si (111) substrates. The peaks at $2\theta = 28.45°$ and 58.86° attribute to Si (111) and Si (222) reflections, respectively. The peaks at $2\theta = 34.05°$ and 71.89° correspond to (0002) and (0004) reflections of InGaN. Also, no secondary phases or residual indium or InN phases were found, confirming that the films are single crystalline. The In composition was determined to be 15% from the linear interpolation of the 2θ peak positions of (0002) GaN (34.59°) and (0002) InN (31.22°). It is clear from the x-ray rocking curves (XRC) as shown in Fig. 1(b) that the FWHM value (deg) of asymmetric reflection (2.16) is higher than that of the symmetric reflection (2.05), which attributes to the presence of large edge threading dislocations (TDs).[15]

The room temperature PL spectra of the $In_xGa_{1-x}N$ films are shown in Fig. 2. Near band edge emission peaks are observed at 502.12 nm corresponding to the bandgap of 2.46 eV. Due to stoke shift of the PL spectra and the discrepancies in the exact value of InN bandgap,[16] there is a lot of ambiguity in exact In content determination from PL spectra. A small hump is observed around 425 nm, which might be due to the initial layers with large number of dislocations arising due to the large lattice mismatch of Si and InGaN films.[17] One can also correlate the presence of large number of defects from the FWHM values of both symmetric and asymmetric XRCs. The low contrast region at the interface, as shown in Fig. 3, most likely attributes to the initial Ga rich InGaN layers corresponding to the ~425 nm peak observed in PL spectra. The thickness was estimated to be ~100 nm from the TEM image. The other dark regions are

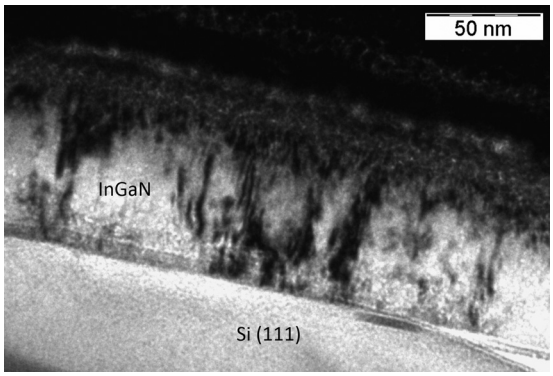

FIG. 3. Cross-sectional transmission electron micrograph of InGaN/Si (111) heterojunction.

formed as a result from the Ga ion beam damage during sample thinning.

Room temperature *I-V* measurements were performed on InGaN/Si (111) heterojunctions with Si biased positively and is shown in Fig. 4. From Fig. 4, it is observed that the device is showing rectifying characteristics, both in the dark (room temperature as well as low temperature) and under ultraviolet radiation, which are consistent with the n-n isotype heterojunctions of other materials as reported by others.[6,7,18] *I-V* characteristics were obtained on Al/InGaN/Si(111)/Al, Al/InGaN/Al, and Al/Si (111)/Al. The behavior of Al/InGaN/Al and Al/Si (111)/Al was ohmic and that of the Al/InGaN/Si (111)/Al junction was rectifying, thus confirming that the rectifying characteristic is primarily arising from the n-InGaN/n-Si isotype heterojunction. Although it seems to be like a leaky rectifying behavior, subsequent low temperature current-voltage measurements were carried out to further confirm the rectifying behavior. Hall measurements were carried out and negligible changes were

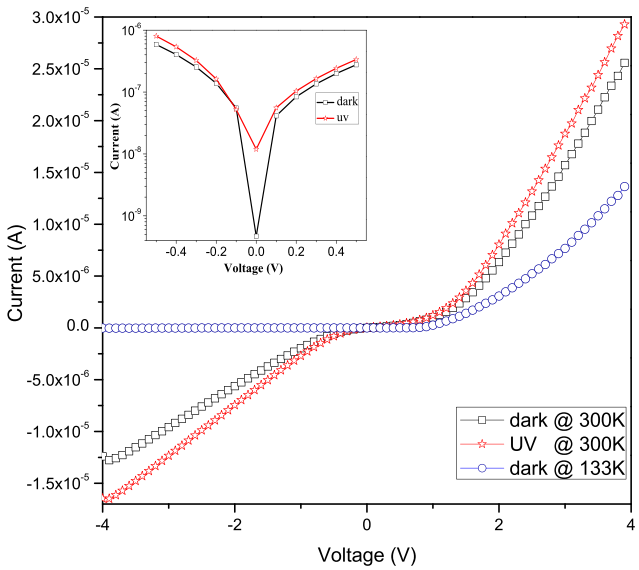

FIG. 4. (a) Typical room temperature current voltage characteristics of n-InGaN/n-Si (111) heterojunction in dark at room temperature (black open squares) and at 133 K (blue open circles), and under UV radiation at room temperature (red open stars). Semi-log plot is shown in inset.

observed at low temperatures in conductivity, mobility, carrier concentration, etc. The room temperature conductivity, mobility, and bulk carrier concentration of the InGaN layer were found to be $\sim$201 $(\Omega\ \text{cm})^{-1}$, $\sim$17 $\text{cm}^2/\text{V s}$, and $\sim 8 \times 10^{19}\,\text{cm}^{-3}$. The excess background electron concentration ($\sim 10^{19}$–10^{21}) is a well observed characteristic of the undoped InGaN and InN due to the nitrogen vacancies in the bulk and along the edge dislocations at the interface and In vacancy/N antisite complexes,[19] which explains the source of doping in our case.

To understand the working of these heterojunctions, it is important to develop a band diagram as shown in Fig. 5(a). χ_1 and χ_2 are the electron affinities of InGaN and Si. The value of χ_2 is well known to be $\sim$4.05 eV. The value of χ_1 is taken as 4.75 eV as per theoretical calculations.[8] Therefore, the conduction band of InGaN lies below the conduction band of Si ($\chi_1 > \chi_2$) and the valence band of InGaN lies below the Si valence band, resulting in the formation of a staggered type heterojunction. For the junction to be in equilibrium as shown in Fig. 5(b), the Fermi levels of both the semiconductors should be aligned. Therefore, electrons from Si flow towards InGaN resulting in the formation of accumulation region on InGaN side and depletion region on the Si side. From the electron affinity values, it can be noted that the conduction band offset is lower as compared to other systems,[7] resulting in lesser band bending and hence the heterojunction exhibits a poorly rectifying behavior at room temperature. At the low temperatures, however, the rectification is relatively improved due to the decrease in thermally generated carrier tunneling. Due to the large lattice mismatch (>11%) between InGaN system and Si (111), the rectifying characteristics cannot be explained by the model proposed by Anderson,[20] since Andersons' model is only applicable to the material systems with no lattice mismatch or less than 1% and also defect free interfaces unlike in the present case, where the presence of a large number of dislocations was confirmed from the HRXRD rocking curves and PL spectra. Huang *et al.*[21] have shown the possible formation of band like deep level traps in the interfacial region between GaN and SiC which suffers from a lattice mismatch of 3.4%. Therefore, it is very likely and inevitable that similar kind of band like deep level traps exist at the interface and strongly alter the behavior of largely lattice mismatched heterojunctions in our case.

The forward bias characteristics of this n-n heterojunction as shown in Fig. 6 are similar to that of a metal-semiconductor junction, considering InGaN as a metal. Therefore, in the forward bias condition, the conduction band of Si rises thereby lowering the barrier height for the electron to flow from Si to InGaN. The forward characteristics can be explained by the Schottky diode equation

$$I = I_s \exp\left(\frac{q(V - IR_s)}{\eta kT}\right), \tag{1}$$

$$\text{with}\quad I_s = AA^*T^2 \exp\left(\frac{-\varphi_b}{kT}\right), \tag{2}$$

where I_s is the saturation current, q is the electron charge, R_s is the series resistance, η is the ideality factor, k is the

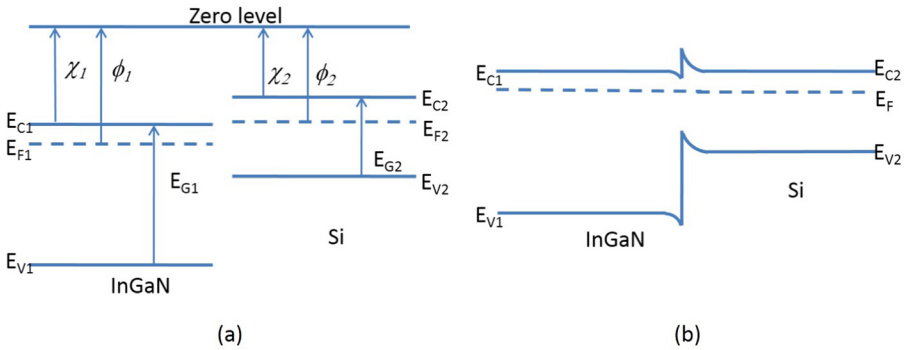

FIG. 5. (a) Schematic energy band diagrams of InGaN and Si before in contact; (b) Equilibrium.

Boltzmann constant, T is absolute temperature, A is the diode area, A^* is the Richardson constant of n type Si (112 A cm^{-2} K^{-2}), and φ_b is the Schottky barrier height. The active diode area is 0.25 cm^2, and the theoretical Richardson constant of Si was taken as 112 A cm^{-2} K^{-2}. The values of φ_b and η, obtained by fitting the forward bias curve using Eq. (1) are 0.82 eV and 11.2. Such high ideality factors arise due to the inhomogeneous interface as a result of interface defects or compositional variations.[22,23] The presence of defect states gives rise to other transport phenomenon and therefore the analysis of Log-Log plots reveals that the conduction mechanism in forward bias is strongly modulated by the interface traps. The Log-Log plot as shown in the inset of Fig. 6 shows three distinct regions assigned as regions I, II, and III depending on the applied voltage. Region I shows a near linear dependence ($I \sim V$) of current on applied voltage which attributes to thermally assisted carrier tunneling. Region II, which corresponds to recombination-tunneling mechanism and is observed in many wideband gap semiconductors,[24,25] follows the relation $I \sim \exp(\alpha V)$, where α is given by Ref. 26 as

$$\alpha = \frac{8\pi}{3h}\left(\frac{m_e^* \varepsilon_{Si}}{N_d}\right)^{1/2}, \tag{3}$$

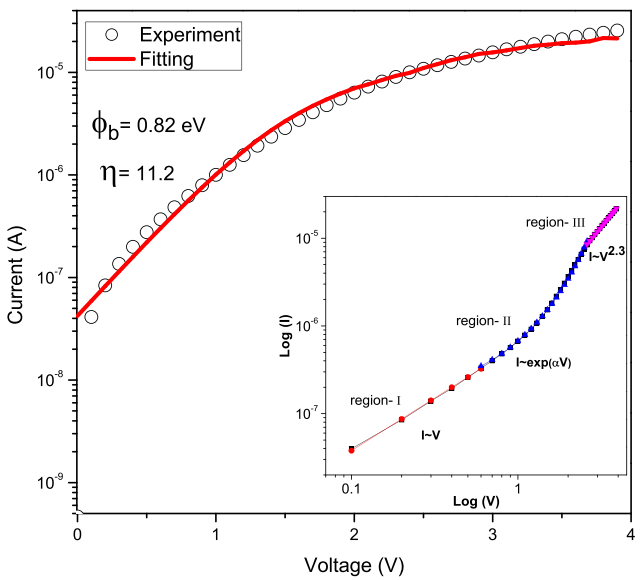

FIG. 6. The forward bias experimental curves (black open circles) fitted with Schottky diode equation (red line). Log-Log plot of current-voltage characteristics under forward bias in inset.

where m_e^* is electron effective mass, ε_{Si} is the permittivity of Si, and N_d is donor density.

The value of α obtained from the fitting is 1.64 V^{-1}, which resembles a low carrier injection situation.

The region III is attributed to Mott-Gurney law given as $I \sim V^m$ $(m \geq 1)$,[27] occurs when injected carrier density is larger than intrinsic carrier density. In this case, the value of m is 2.3, greater than 2 (ideal Mott-Gurney characteristic), which may be due to the exponential trap distribution as observed by Kumar *et al.*[28] The current voltage characteristics in this region can be explained by the trapping model[29,30]

$$I = Aq^{1-l}\mu_n N_c \left(\frac{2l+1}{l+1}\right)^{l+1}\left(\frac{l}{l+1}\frac{\varepsilon_s\varepsilon_0}{H_b}\right)^{l}\frac{V^{l+1}}{d^{2l+1}}, \tag{4}$$

where A is the area of the device, q is the elementary charge, μ_n is the mobility of the material, N_c is the density of states in conduction band, ε_s is permittivity of the material, ε_0 is free space permittivity, H_b is density of traps, V is applied voltage, d is the thickness of epilayer, and l (>1) is given as

$$l = \frac{E_t}{k_b t} = \frac{T_c}{T}, \tag{5}$$

since $E_t = k_b T_c$, where T_c is the characteristic temperature of traps, E_t is the characteristic trap energy at temperature T_c, and k_b is Boltzmann constant. The values of all the parameters used in fitting are $l = m - 1$, i.e., 1.3, $A = 0.25\,cm^2$, $\mu_n = 17\,cm^2/V\,s$, $N_c = 6.4838 \times 10^{23}\,cm^{-3}$, $\varepsilon_s = 10.5$ F/cm, $\varepsilon_0 = 8.85 \times 10^{-14}$ F/cm, $d = 0.125 \times 10^{-4}$ cm, and $H_b = 5.5 \times 10^{20}\,cm^{-3}$. Therefore, we can strongly believe that at and above room temperature, the forward current mainly does not flow over the barrier, instead flows along a defect path formed due to the large concentration of dislocations arising due to large lattice mismatch. Similar kind of behavior has been observed in n-GaN/n-6H-SiC heterojunctions[21] and also in InAs/AlSb n-n heterojunctions.[31] The calculated trap or space charge densities in case of n-GaN/n-6H-SiC heterojunction having a lattice mismatch of 3.51% was found to be in the order of $\sim 10^{20}\,cm^{-2}$, which correspond to dislocation density of $\sim 10^{12}\,cm^{-3}$ and in our case the obtained trap densities due to a much larger lattice mismatch of ~17% seem to be totally justified. In both the above mentioned systems, the transport across the heterojunction is defect mediated with lattice mismatch <10%. Therefore, it provides a strong reference for the defect assisted transport in our case.

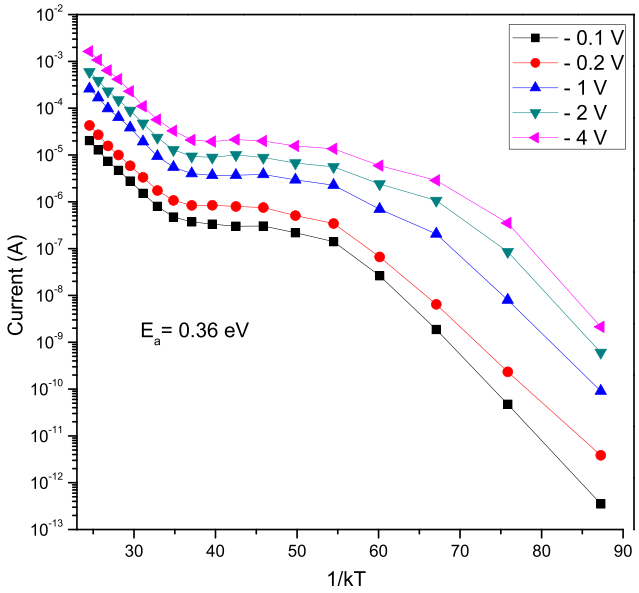

FIG. 7. Arrhenius plot of temperature dependent characteristics at several reverse biases.

In the reverse bias condition, i.e., when electric field is applied to InGaN, the leaky reverse bias behavior is observed and attributed to the defect assisted transport, which is observed in many wide bandgap semiconductors. In a perfectly lattice matched and defect free heterojunction, the barrier height increases with the increase in reverse bias preventing the current flow. At sufficiently high bias, the increase in barrier height results in thinning of the barrier which makes the charge carriers tunnel to other side through the barrier. In the present case, due to the presence of large threading dislocations at interface, the most likely conduction mechanisms may be trap assisted tunneling or Variable Range Hopping (VRH).[32] The Arrhenius plot of temperature dependent current-voltage data indicates the presence of trap levels as shown in Fig. 7. The activation energy obtained from the slope is 0.36 eV. However, the defect structure formed at the interface may be complex and needs a further detailed study to determine the exact nature of defects and their impact on carrier transport behavior.

Although the device is not perfectly rectifying at room temperature, the interesting characteristics observed were in the region of zero bias. An abrupt increase in photocurrent in the presence of UV radiation was observed at zero bias than either reverse or positive biases and is shown in the inset of Fig. 4. Ager *et al.*[8] have shown the operation of similar devices in photovoltaic mode. However, the InGaN films grown on their samples were much thicker compared to the present work and also used several buffer layers. The photocurrent response and stability were studied from the on-off cycles of a UV lamp at zero bias and different voltages and is shown in Fig. 8(a). The order of increase in the photocurrent magnitude is higher in case of zero bias (>1.5) than that of the positive and reverse bias. Fig. 8(b) shows the growth and decay responses which can be described as[33]

$$I(t) = I_{dark} + A\left[1 - \exp\left\{\frac{-(t-t_0)}{\tau_g}\right\}\right], \quad \text{and} \qquad (6)$$

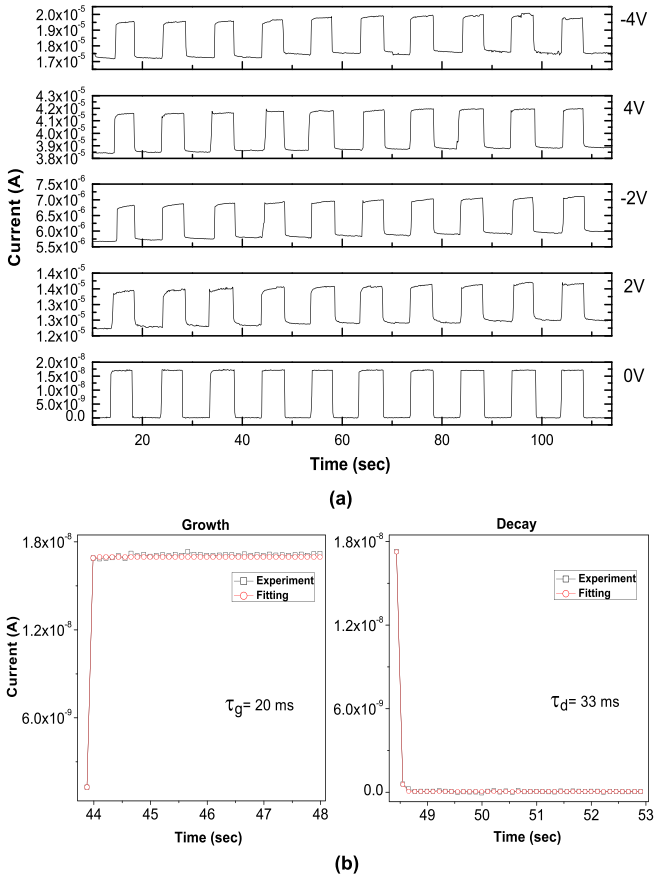

FIG. 8. (a) Photoresponse of device at different working voltages. (b) Time response of photocurrent growth and decay from the fitting (red line) of experimental values (black open squares).

$$I(t) = I_{dark} + A\left[1 - \exp\left\{\frac{-(t-t_0)}{\tau_d}\right\}\right], \qquad (7)$$

for growth and decay, respectively, where I_{dark} is the dark current, A is the scaling constant, t_0 is the time when UV lamp was switched on or off for growth or decay, respectively, and τ_g and τ_d are growth and decay times. The response times obtained from the above equations are 20 ms and 33 ms for growth and decay. The responsivity (R_λ) of this photodetector is calculated from $R_\lambda = \frac{I_\lambda}{P_\lambda S}$, where I_λ is the photocurrent, P_λ is the incident power of UV lamp of wavelength λ, and S is the area of illuminated junction which is 0.09 cm^2. The External Quantum Efficiency (EQE) is given as $EQE = \frac{hcR_\lambda}{e\lambda}$.[34] The values obtained for spectral responsivity and external quantum efficiency are 0.0942 A/W and 32.4%, respectively, which are better than the values reported in the literature[10] for such devices. The responsivities and external quantum efficiencies in case of different biases were found to be better than zero bias (Table I). From Fig. 8(a), it can be seen that the photocurrent obtained at different biases do not overlap, i.e., the photocurrent range in each case is distinct from that of the others, suggesting that such devices can be used for switching purposes and logical operations as well.

The mechanism for this type of behavior in n-n isotype heterojunctions can be explained with the help of a model proposed by Yawata and Anderson.[2] When the electron and

TABLE I. Responsivities and external quantum efficiencies of the photodetector at different bias.

Working voltage (V)	Responsivity (A/W)	External quantum efficiency (%)
0	0.0942	32.4
2	0.6217	213.8
4	1.7097	588.1
−2	0.5746	197.6
−4	1.2575	432.5

hole pairs are generated, the electrons are swept away from the junctions due to the built-in-electric field, whereas the holes are trapped in the notch. The holes being positively charged, neutralize the electrons at interface, and eventually lower the barrier height. For an intense illumination, the concentration of holes trapped at the notch is increased, thus drastically lowering the barrier height and result in abrupt increase of electron flow. However, in case of a bias (positive or negative—as explained above), the electrons at the interface tunnel through the depletion region leaving behind holes which are eventually refilled by electrons from the other side. The forward and negative bias characteristics from the current voltage plots are in good agreement with the proposed mechanism.

IV. CONCLUSIONS

In summary, we have successfully grown InGaN thin epilayers directly on bare n-Si (111) without any buffer layer or nitridation steps by plasma assisted molecular beam epitaxy. The electrical characteristics of the n-InGaN/n-Si (111) isotype heterojunctions were analyzed and studied thoroughly. It was found that the current transport mechanisms were largely driven by the interface defects and the trap density was found to be $5.5 \times 10^{20}\,\mathrm{cm}^{-3}$. Photodetection studies were carried out using a UV lamp and we successfully demonstrated long UV photo-response characteristics with response times less than 100 ms, responsivity of 0.0942 A/W, and external quantum efficiency of 32.4% at zero bias. Although the response times are relatively large in magnitude, the discrete response characteristics at zero bias make it a self-powered UV photodetector. The device showed consistent response over a period of 6 months. Since the trick lies at the interface of the heterojunction, the degradation of response is expected to be very slow over the period of time and thus makes it robust and reliable. Such self-sustainable and environmental friendly devices will eventually reduce energy requirements.

[1]H. Y. Kim, J. H. Kim, Y. J. Kim, K. H. Chae, C. N. Whang, J. H. Song, and S. Im, Opt. Mater. **17**, 141 (2001).
[2]S. Yawata and R. L. Anderson, Phys. Status Solidi **12**, 297 (1965).
[3]S. T. Tan, X. W. Sun, J. L. Zhao, S. Iwan, Z. H. Cen, T. P. Chen, J. D. Ye, G. Q. Lo, D. L. Kwong, and K. L. Teo, Appl. Phys. Lett. **93**, 013506 (2008).
[4]M. K. Hudait and S. B. Krupanidhi, J. Vac. Sci. Technol. B **17**, 1003 (1999).
[5]A. G. Milnes, Solid-State Electron. **29**, 99 (1986).
[6]T. L. Tansley and S. J. T. Owen, J. Appl. Phys. **55**, 454 (1984).
[7]A. K. Srivastava, J. L. Zyskind, R. M. Lum, B. V. Dutt, and J. K. Klingert, Appl. Phys. Lett. **49**, 41 (1986).
[8]J. W. Ager, L. A. Reichertz, Y. Cui, Y. E. Romanyuk, D. Kreier, S. R. Leone, K. M. Yu, W. J. Schaff, and W. Walukiewicz, Phys. Status Solidi C **6**, S413 (2009).
[9]P. Kumar, P. E. D. S. Rodriguez, V. J. Gómez, N. H. Alvi, E. Calleja, and R. Nötzel, Appl. Phys. Express **6**, 035501 (2013).
[10]S. M. Hatch, J. Briscoe, and S. Dunn, Adv. Mater. **25**, 867 (2013).
[11]Y. Q. Bie, Z. M. Liao, H. Z. Zhang, G. R. Li, Y. Ye, Y. B. Zhou, J. Xu, Z. X. Qin, L. Dai, and D. P. Yu, Adv. Mater. **23**, 649 (2011).
[12]L. S. Chuah, Z. Hassan, and H. Abu Hassan, Microelectron. Int. **25**, 3 (2008).
[13]J. Ohsawa, T. Kozawa, O. Fujishima, and H. Itoh, Phys. Status Solidi C **3**, 2278 (2006).
[14]M. Kumar, B. Roul, M. K. Rajpalke, T. N. Bhat, A. T. Kalghatgi, and S. B. Krupanidhi, Curr. Appl. Phys. **13**, 26 (2013).
[15]B. Heying, X. H. Wu, S. Keller, Y. Li, D. Kapolnek, B. P. Keller, S. P. DenBaars, and J. S. Speck, Appl. Phys. Lett. **68**, 643 (1996).
[16]G. Orsal, Y. El Gmili, N. Fressengeas, J. Streque, R. Djerboub, T. Moudakir, S. Sundaram, A. Ougazzaden, and J. P. Salvestrini, Opt. Mater. Express **4**, 1030 (2014).
[17]J. Wu, W. Walukiewicz, K. M. Yu, J. W. Ager, E. E. Haller, H. Lu, and W. J. Schaff, Appl. Phys. Lett. **80**, 4741 (2002).
[18]A. G. Milnes and W. G. Oldham, Solid-State Electron. **6**, 201 (1963).
[19]B. N. Pantha, H. Wang, N. Khan, J. Y. Lin, and H. X. Jiang, Phys. Rev. B **84**, 075327 (2011).
[20]R. L. Anderson, Solid-State Electron. **5**, 341 (1962).
[21]Y. Huang, X. D. Chen, S. Fung, C. D. Beling, C. C. Ling, X. Q. Dai, and M. H. Xie, Appl. Phys. Lett. **86**, 122102 (2005).
[22]M. W. Allen and S. M. Durbin, Appl. Phys. Lett. **92**, 122110 (2008).
[23]S. Bayan and D. Mohanta, J. Appl. Phys. **110**, 054316 (2011).
[24]T. N. Bhat, M. K. Rajpalke, B. Roul, M. Kumar, and S. B. Krupanidhi, J. Appl. Phys. **110**, 093718 (2011).
[25]S.-Y. Liu, T. Chen, Y.-L. Jiang, G.-P. Ru, and X.-P. Qu, J. Appl. Phys. **105**, 114504 (2009).
[26]D. Song and B. Guo, J. Phys. D: Appl. Phys. **42**, 025103 (2009).
[27]A. Rose, Phys. Rev. **97**, 1538 (1955).
[28]V. Kumar, S. C. Jain, A. K. Kapoor, J. Poortmans, and R. Mertens, J. Appl. Phys. **94**, 1283 (2003).
[29]A. K. Kapoor, S. C. Jain, J. Poortmans, V. Kumar, and R. Mertens, J. Appl. Phys. **92**, 3835 (2002).
[30]M. Kumar, B. Roul, A. Shetty, M. K. Rajpalke, T. N. Bhat, A. T. Kalghatgi, and S. B. Krupanidhi, Appl. Phys. Lett. **99**, 153114 (2011).
[31]A. Nakagawa, H. Kroemer, and J. H. English, Appl. Phys. Lett. **54**, 1893 (1989).
[32]E. J. Miller, E. T. Yu, P. Waltereit, and J. S. Speck, Appl. Phys. Lett. **84**, 535 (2004).
[33]S. Ghosh, B. K. Sarker, A. Chunder, L. Zhai, and S. I. Khondaker, Appl. Phys. Lett. **96**, 163109 (2010).
[34]B. Chitara, S. B. Krupanidhi, and C. N. R. Rao, Appl. Phys. Lett. **99**, 113114 (2011).